Journal of Materials Science: Materials in Medicine (2025)36:89
https://doi.org/10.1007/s10856-025-06954-8

DELIVERY SYSTEMS

Original Research

Evaluation of biological functionality of biomaterial surface modified by advanced laser equipment

Inho Bae[1,2] · Ik-Bu Sohn[3] · Byung-Hoon Kim[1,2]

Received: 19 March 2025 / Accepted: 28 September 2025

Abstract

The study presents a novel high focus laser scanning (HFLS) system, which integrates the advantages of conventional equipment, and demonstrates its superiority. The biological functions of biomaterial surfaces modified using HFLS were investigated. The advantages of HFLS, including ease of use, processing speed, and precision, were validated via morphological analyses such as microscopy, and surface characterization techniques such as contact angle measurements. The material surfaces were modified into the 'Line' and the 'Grid' shapes to facilitate further investigations on cellular response and drug delivery. Cell adhesion, migration, and proliferation were examined to investigate cellular responses to HFLS-modified material surfaces. To evaluate the functionality of HFLS-modified materials as drug carriers, prednisolone (PDS) holding capacity, drug release, platelet adhesion, and western blot analysis for inflammatory cytokines were performed. Compared with conventional methods, HFLS processing proved to be faster and more precise, enabling easy modification of materials into hydrophilic (the Line) or hydrophobic (the Grid) surfaces. The highest contact angle ($158.63° \pm 1.26$) was observed for surfaces processed with a 50 μm wave size. Cell culture medium spread across nearly the entire surface on the Line compared to the control, whereas minimal spread was observed on the Grid. These results align with those of cell adhesion, migration, proliferation, and platelet adhesion assays. Moreover, HFLS-modified materials demonstrated increased PDS retention, with PDS release occurring in a controlled manner rather than disappearance due to rapidly drug eluted. The released PDS maintained an anti-inflammatory effect, reducing the expression of cytokines associated with M1 macrophages. The laser system presented in this study proposes a promising approach for enhancing tissue engineering applications, including surface morphology modification, cytocompatibility improvement, and efficient drug delivery. Additionally, it holds potential for clinical accessibility as an equipment owing to its versatility.

✉ Inho Bae
ihbae@chosun.ac.kr

✉ Byung-Hoon Kim
kim5055@chosun.ac.kr

[1] Department of Dental Materials, College of Dentistry, Chosun University, 7 Chosundaegil, Dong-gu, Gwangju, Republic of Korea

[2] Convergence research center for treatment of oral soft tissue disease (MRC), College of Dentistry, Chosun University, Gwangju, Republic of Korea

[3] Advanced Photonics Research Institute, Gwangju Institute of Science and Technology, Gwangju, Republic of Korea

Published online: 14 October 2025

Graphical Abstract

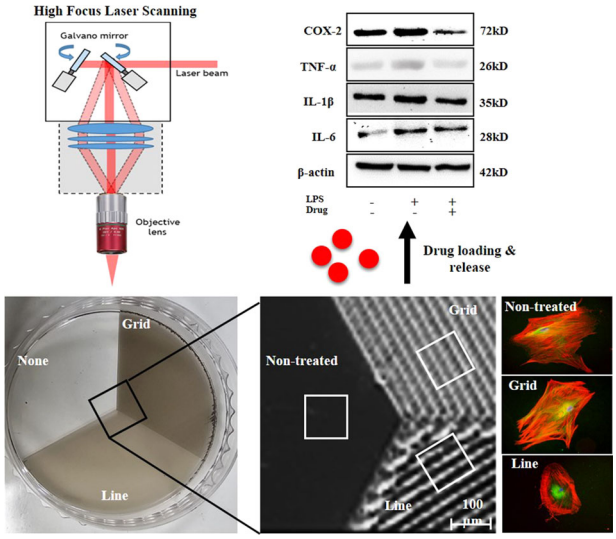

1 Introduction

Recent advancements in tissue engineering have emphasized the importance of surface properties of biomaterials, as these significantly influence cell responses [1], corrosiveness [2], biocompatibility [3], drug delivery [4], and functional enhancement [5]. Various surface modification techniques have been explored. These include hydrothermal treatment [6, 7], reactive ion etching [8, 9], electropolishing [10], anodic oxidation [11], and laser irradiation [12]. However, surface modification by chemical methods such as electropolishing and anodizing pose challenges in controlling specific parameters, including surface roughness, reproducibility of surface features, and uniformity of oxide layer thickness. Moreover, these techniques typically involve harsh chemicals such as hydrofluoric acid, which can adversely affect the cellular response [13]. In contrast, surface modification using femtosecond lasers (FSLs), as discussed in our previous study, offer several advantages. These include ease of operation compared with that of other methods, immunity to thermal, mechanical, and chemical influences, and consistent results [14]. Owing to these advantages, FSLs have gained traction in clinical fields, including contrast sensitivity assessment [15], intracellular nanosurgery [16], and cell perforation via plasmonic bubbles [17]. A notable benefits of FSLs in clinical applications is their high cutting precision, which facilitate delicate procedures with minimal collateral damage. Additionally, surface patterning using FSLs can regulate cell migration and repellency [18]. Despite these advantages, conventional FSL present limitations that need to be addressed. For instance, the objective lens method enables precision processing but operates at a relatively low speed. Conversely, the scanning method enables high-speed operations but lacks sufficient precision. These trade-offs have been reported in previous studies investigating femtosecond laser-based surface processing [15, 16].

To address these limitations, this study developed a high-focus laser scanning (HFLS) system designed to complement and improve the capabilities of conventional FSLs [19]. The study aimed to process material surfaces for specific applications using HFLS and to evaluate the performance of the modified material.

The regeneration of tissues by implanting biomaterials in areas of the human body with functional impairments is well established. In the dental field, chronic conditions such as periodontitis and peri-implantitis present significant treatment challenges. Notably, following dental implantation, peri-implantitis negative impacts tissue recovery, frequently resulting in poor prognosis and necessitating reoperation. Consequently, clinical challenges persist in areas such as suppressing bacterial infiltration around the implant crown, managing inflammation at the screw interface, and promoting soft tissue regeneration. Furthermore, biomaterial implanted in various regions of the human body are exposed to local environmental factors, including blood reactions [20] and tissue compatibility [21]. Therefore, the surface properties of biomaterials can lead to negative clinical prognosis, such as thrombosis and inflammation [22, 23]. Because inflammation suppression is a key factor in healing damaged tissue, local drug delivery systems aimed at alleviating inflammation are considered an effective approach. Therefore, drug delivery is an important factor in evaluating the functional superiority of

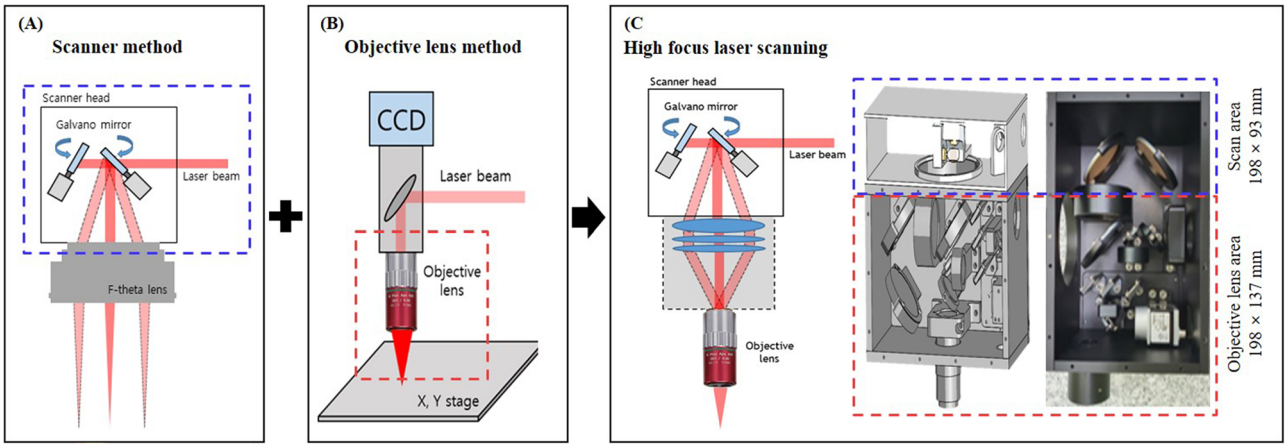

Fig. 1 Schematic diagram of HFLS fabrication. By applying relay optics to the areas of scanning method (**A**) and objective lens method (**B**), the two conventional equipment are independently combined to present the three-dimensional and real images of the device (**C**). The blue dotted box indicates the scanning area, and the red dotted box indicates the objective lens area

biomaterials. Several studies have previously explored both surface modification by physical methods such as polymer coating [24], irradiation of ion beam [25], FSLs irradiation [14], and microporosity [26], as well as surface modification by chemical methods such as anodizing [27], electropolishing [10], and plasma treatment [28, 29], for effective drug delivery of biomaterials. Foreign substances, such as bacteria and implants, can significantly affect cellular behavior because cell is sensitive to their surroundings. In particular, sequential cellular responses such as cell signaling, adhesion, migration, elongation, proliferation, differentiation and cytoskeletal changes during these processes can be altered by the physical properties of the biomaterial interface, such as the material surface topography [30]. The surface properties, such as chemistry, wettability, and topography [31] are important factors in the Interfacial interactions between biomaterial surface and surrounding tissues. It could determine the initial cellular responses and eventually influence cell fate [32]. Therefore, the surface character of biomaterial can be controlled by using the HFLS technique proposed in this study, facilitating the implementation of specific functions for clinical applications. Furthermore, modification of material surface has been demonstrated to enhance the functionality of biomaterial by controlling the amount and release rate of drugs [14]. Various drugs, including prednisolone (PDS) [33], everolimus [34], artemisinin [35], and peptides [36] have been utilized to assess the drug delivery potential and efficacy of modified biomaterial surfaces. PDS, a synthetic glucocorticoid cortisol derivative, is typically used to treat inflammatory and autoimmune diseases and has demonstrated positive anti-inflammatory effects in previous studies [37]. Therefore, the aims of this study was to evaluate the surface properties of biomaterials to create hydrophobic or hydrophilic surfaces and verify the subsequent cellular responses, thereby simulating clinical applications using the newly developed HFLS technique. Additionally, the efficacy of PDS delivery and the performance of surface-modified materials in facilitating drug delivery were investigated.

2 Materials and methods

2.1 Fabrication of high focus laser scanning

In this study, a new type of HFLS equipment (Fig. 1C) was fabricated by combining the advantages of high-speed processing employing the scanner method (Fig. 1A) with high-focus precision processing employing the objective lens method (Fig. 1B). The scanning area was 198 × 93 mm and the objective lens area was 198 × 137 mm [19].

2.2 Surface modification

The performance of the HFLS system was compared with that of conventional equipment by irradiating the surfaces of various materials such as silicon (Si) wafer, silica, and printed circuit boards (PCB). Polystyrene (PS, 30 mm in diameter), the most suitable material for cell culture, was used to evaluate the effect of material surface modified by HFLS on cellular responses. The samples were divided into three groups: (1) None (non-treated), (2) Line, and (3) Grid (cross-Line). Additionally, the HFLS was irradiated. The Line was irradiated once with the HFLS, and the Grid was irradiated once more along the cross-axis following Line irradiation. HFLS irradiation was performed at conditions of 1030 nm of wavelength, 700 mW of power, 100 mm/s of speed, 100 kHz of frequency, and 250 femtosecond of pulse duration.

2.3 Morphological analysis

The surface of the laser-irradiated biomaterial and platelet were visualized by scanning electron microscopy (SEM; Hitachi, Tokyo, Japan) under 5 ~ 15 kV. For the platelet imaging, the specimen was sputter-coated with platinum, fixed with glutaraldehyde (2.5%) for 2 h, and then dehydrated sequentially by increasing the ethanol concentration from 40 ~ 100%. Thereafter, ethanol was evaporated for 24 h and subjected to SEM analysis. The average number of platelets on the material surface was calculated by randomly selecting ten sectors.

2.4 Investigation of surface property

The surface properties of the HFLS-modified materials were investigated by measuring the surface contact angle. Measurements were conducted using GSX (Surfacetech, Gwangju, Korea) with both imaging and surface contact angle measurements performed using Surfacetech (version 1.1.5.6) software. Average values from three independent experiments are presented.

2.5 Cell culture

This study was performed to simulate an experimental approach for peri-implantitis using human gingival fibroblasts (HGF). The cell was cultured in Dulbecco's modified Eagle's medium containing with fetal bovine serum (10%) and penicillin (1%) in CO_2 atmosphere (5%) at 37 °C.

2.6 Fluorescence microscopy analysis

After culturing the cell on the HFLS-modified material surface for 4 h, the morphology of initial focal cell adhesion was examined via fluorescence microscopy. For fluorescence microscopy, cell was fixed with paraformaldehyde (4%, SM-P01-050, SolMateTM, Gene All Biotechnology, Seoul, Korea) for 15 min, permeabilized with Triton X-100 (0.5%, T8787, Sigma, St. Louis, MO, USA) for 10 min, and blocked with bovine serum albumin (2%, BSA, A9647; Sigma, St. Louis, MO, USA) for 30 min. After washing several times with phosphate buffered saline (PBS, pH 7.0) to remove non-attached cell, it was incubated with vinculin (1:50, ab129002, Abcam, Cambridge, UK) or Rodamine (2.88 µg/mL, ab216652, Abcam, Cambridge, UK) antibodies at 4 °C for 24 h. Subsequently, the cell was incubated with Alexa Fluor 488 (1:1000, A21206, Invitrogen, ThermoFisher Scientific, Waltham, MA, USA) for 1 h and then mounted with DAPI (H-1500, Vector Laboratories, Newark, CA, USA) and phalloidin (H-1600, Vector Laboratories, Newark, CA, USA) mounting medium (1:1). The surface image was acquired using a Nikon Eclipse Ni-U fluorescence microscope (Nikon, Tokyo, Japan).

2.7 In vitro cellular responses

To determine the extent of cell migration, a scratch test, a validated method previously conducted by our research team, was performed [10]. After seeding cell (1×10^4 cells/cm^2) for 24 h, The middle area of the cell monolayer was scraped manually (using sterile pipette tip in this study, ~12.0 ± 1.05 mm^2) to create a cell-empty space of ~50 µm width. After culturing the cells for 24 h, a randomly selected region of interest was imaged in the scratched area was imaged [38]. The rate of cell migration was calculated as 100× [(12.0 ± 1.05 - scraped area not filled with cells after 24 h of incubation)/12.0 ± 1.05]. Proliferation of HGF on PS surfaces modified by HFLS was examined using the WST-1 assay and EZ-cytox reagent (Daeil Research Institute, Seoul, Korea). Briefly, EZ-cytox reagent (40 µL) was added to each well of cell culture dish (24-well). When the color of the reagent turned yellow (~10 min), the amount of dye-detectable formazan metabolized by mitochondrial dehydrogenase of living cells was determined spectrophotometrically by measuring absorbance at 450 nm using a microplate reader (Bio-Tek Instruments, Winooski, VT). The measurements were carried out at a designated duration and the amount of formazan salt formed was expressed as a ratio to the number of viable cells.

2.8 Investigation of platelet adhesion on material surface

A platelet adhesion examination was performed to evaluate the thrombogenic potential of the HFLS-modified material surface, platelet adhesion experiment was performed [39]. Fresh porcine whole blood (45 mL) was mixed with 3.8 wt.% sodium citrate solution (5 mL, 9:1 ratio) and centrifuged at $150 \times g$ for 15 min. The resulting supernatant platelet-rich plasma (PRP) was carefully harvested and centrifuged at $500 \times g$ for 20 min to isolate the platelet pellet. The pellet was dissolved in PRP for subsequent experiments. Platelets were loaded onto the material surface at a density of 5×10^7/mL and incubated for 180 min. The specimen was rinsed three times to remove platelet that were nonspecifically attached to the surface. The morphology and population of platelet on the material surface were examined using SEM.

2.9 Quantification of total drug amount in material surface and release

To quantify the total drug amount in material surface and release from the HFLS-modified material surface, 200 µL of

PDS was dissolved at 5 wt.% in tetrahydrofuran (THF) and loaded on the material surface. Subsequently, the specimen was gently shaken and left undisturbed for 24 h to ensure uniform distribution of PDS across the material surface. The material surface was gently washed with deionized water and freeze-dried as previously described [40]. To determine the maximum amount of PDS that could be injected into the material, the specimen was immersed in a THF solution, gently shaken to release sufficient PDS, harvested, and analyzed using a UV-*vis* spectrometer (Multiskan EX; ThermoFisher Scientific, Waltham, MA, USA). To determine the velocity of PDS released from the material surface, the specimen was immersed in PBS. At every designated time points, the PBS was harvested and the absorbance was measured using a UV-*vis* spectrometer. When the UV value approached zero, the PDS was considered to no further release. The PDS release amount was determined based on the drug standard curve, and the cumulative amount of PDS released from the material surface was expressed as a percentage of the total amount of PDS injected into the material surface.

2.10 Western blotting

Western blot analysis was performed using RAW264.7 macrophages, to investigate the anti-inflammatory effect of PDS released from the material surface. To activate various inflammatory markers in RAW264.7 macrophages, lipopolysaccharide (LPS, 1 μg/mL) was treated and incubated for 1 h. Cell was lysed with RIPA lysis buffer (Cell signaling, Beverly, MA, USA), and protein concentration was measured using a bicinchoninic acid protein assay kit. Twenty microgram of protein was then separated on sodium lauryl sulfate-polyacrylamide gel (10%) and transferred to a polyvinylidene fluoride membrane (Millipore, Bedford, MA). After the membrane was blocked with BSA (5%) for 1 h, the blot was incubated with primary antibodies {(1:1000 in BSA (1.5%)} at 4 °C, followed by horseradish peroxidase-conjugated secondary antibodies (all 1:3000) for 1 h. The cytokine expression pattern was detected using enhanced chemiluminescence (GE Healthcare Biosciences, Piscataway, NJ), expressed cytokine intensity was quantified using Gel-Pro software, and the amount of cytokines expressed was normalized to the intensity of the control and expressed as a fold of control.

2.11 Statistical analysis

All values were analyzed with SPSS software (version 11.0; SPSS Inc., Chicago, IL, USA). The results are expressed as mean ± standard deviation (SD). $*p < 0.05$ and $**p < 0.01$ values were considered statistically significant.

3 Results

3.1 Development of a high-focus laser scanning equipment

This study developed a novel HFLS system that integrates the advantages of the high-speed processing of the scanner method (Fig. 1A) and high-focus precision processing of the objective lens method (Fig. 1B) to process biomaterials quickly and precisely [19]. The laser beam moving radially from the scanner was focused to a single point on the objective lens for even irradiation. To facilitate this, the objective lens area was increased (Fig. 1C) (scan area: 198 mm × 93 mm; objective lens area: 198 mm × 137 mm).

3.2 Comparison of newly developed equipment with conventional equipment

The surfaces of the Si wafer, silica, and PCB were processed using the HFLS, and their efficiencies were compared with those of the conventional equipment. All processes were performed under the specific conditions described earlier. When the surface was processed using the objective lens method, the depths and widths of the Si wafer, silica, and PCB surfaces increased proportionally with the number of processing cycles (Fig. 2A). The surfaces of the Si wafer and silica, processed ~24 times using the objective lens method, exhibited a similar degree of processing to a single application of HFLS. However, PCB required processing more than three times to achieve an efficiency equivalent to that obtained in one processing of HFLS, and satisfactory results comparable to those of HFLS were obtained after processing six times (Fig. 2B).

3.3 Polystyrene surface modification for cell response evaluation

To explore the possibility of applying biomaterials to a HFLS equipment, the surface of PS was modified into the Line and the Grid as described above, and SEM analysis was subsequently performed. Consequently, the PS surface was divided into three sections. A parallel line shape with a specific pattern was observed in the Line, and a pattern consistent with that of the Line was observed in the cross direction and spacing in the Grid. The processing width of each group was ~10 μm and the interval was 20 μm (Fig. 3).

3.4 Characterization of material Surface

The characteristics of material surfaces processed in the Line or the Grid were investigated using HFLS. It was validated via microscopy that each material surface was modified optimally into the desired shape by HFLS (Fig. 4A), and the surface

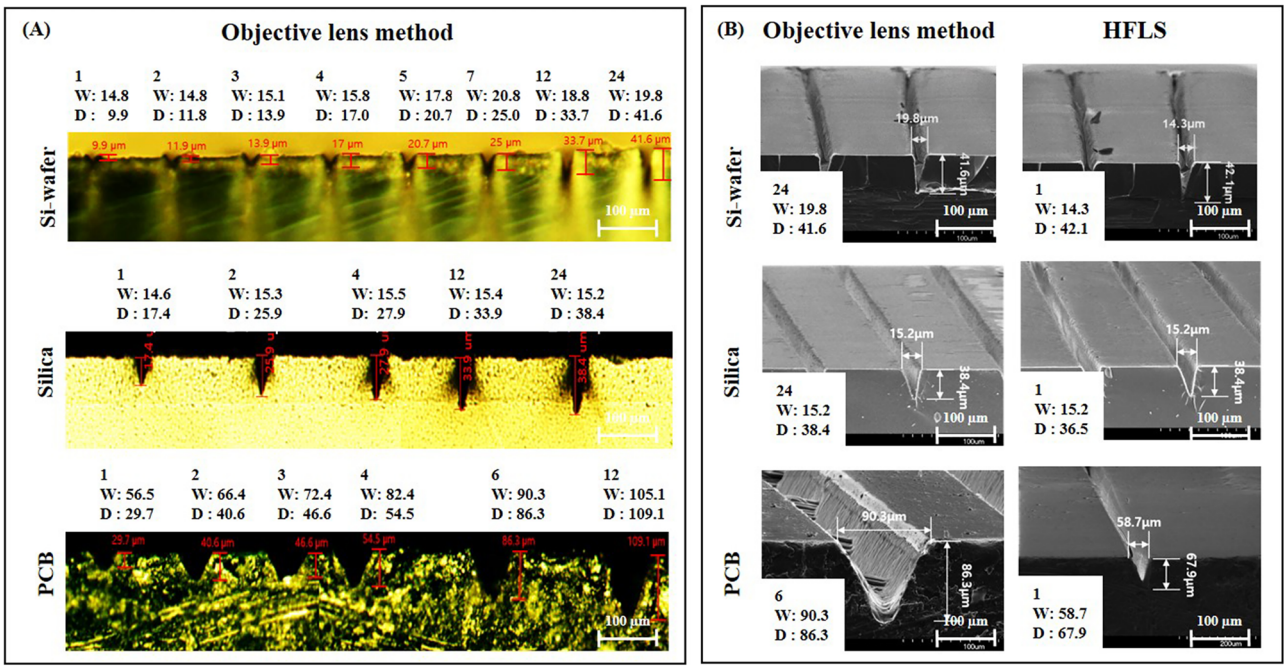

Fig. 2 Comparison of processing efficiency of HFLS with conventional objective lens method. Surface modification change according to the number of treatments for each material using the objective lens method (**A**) and the processing time similar to that of HFLS (**B**) are represented. W, D, and numbers indicate width, depth, and number of processing repetitions, respectively. The unit is μm

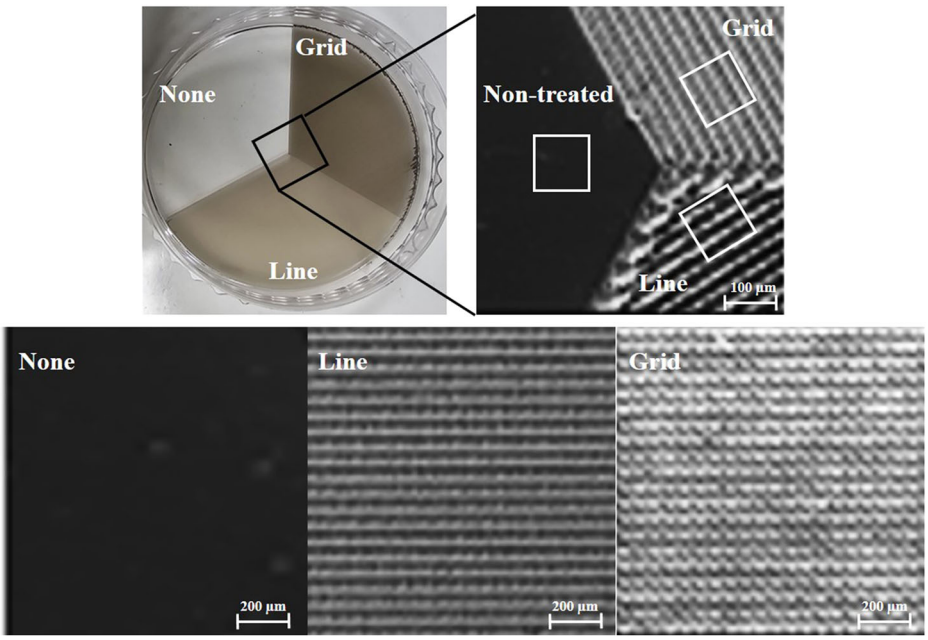

Fig. 3 Morphological analysis for the Line and Grid of PS surface processed with HFLS. PS surface, a material for cell culture, is divided into three areas: None, Line, and Grid, and processed with HFLS. The square box designates the enlarged area

contact angle of the Line was significantly reduced (hydrophilicity) compared to that of the None case (None; 73.3° ± 2.85 vs. Line; 6.9° ± 3.42, respectively, $p < 0.01$). Concurrently, the contact angle of the Grid increased significantly (hydrophobicity) compared to that of the untreated group (None; 73.3° ± 2.85 vs. Grid; 100.6° ± 5.66, respectively, $p < 0.01$) (Fig. 4B). These surface characteristics were also consistent with those of dental implants used clinically (Fig. 4C). The effect of the wave size was investigated when the material surface was modified into a grid shape using an HFLS to induce hydrophobicity. Consequently, the grid-shaped material surface (Fig. 5A) resulted in an increased contact angle (hydrophobic), and the surface contact angle continued to increase with wave size, initial value being 30 μm (142.9° ± 0.35), and the highest contact angle was exhibited at the wave size of 50 μm (158.63° ± 1.26). Thereafter, the

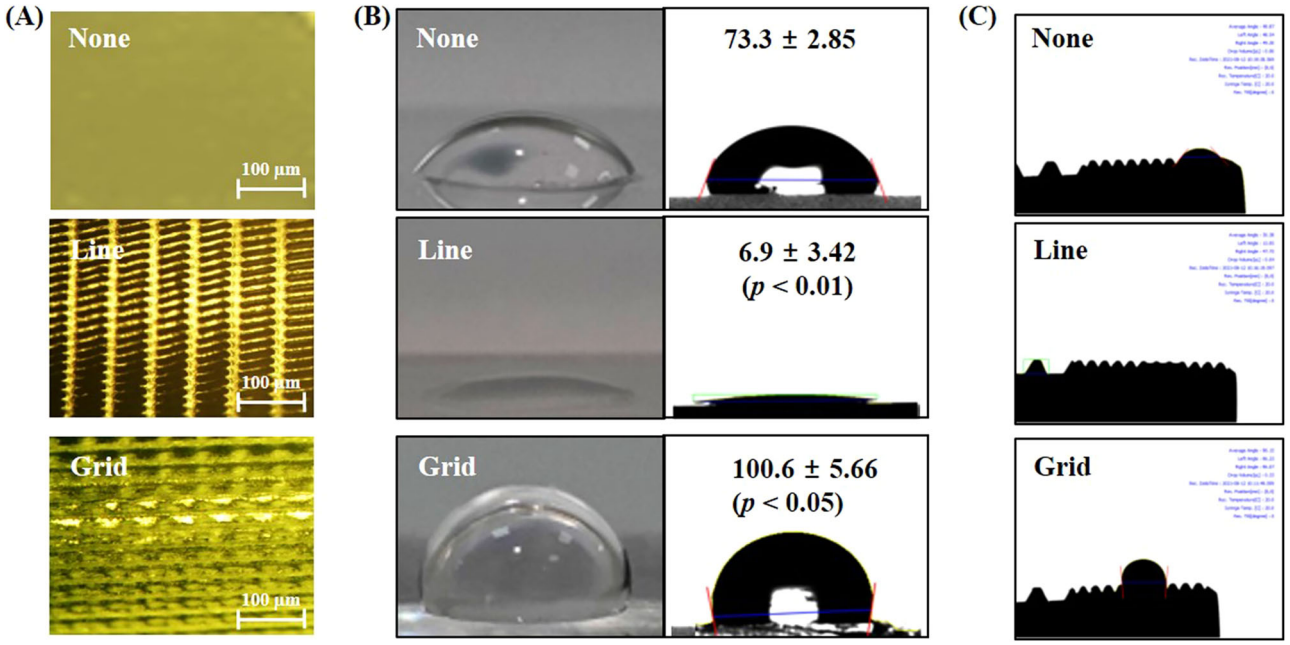

Fig. 4 Comparison of characteristics of modified material surface. Optical images of the material surface (**A**), the surface contact angle of two-dimensional titanium (**B**), and the three-dimensional dental implant modified by HFLS (**C**) are represented. The indicated values are means ± SD ($n = 3$). *P* values are statistical values compared to the None case

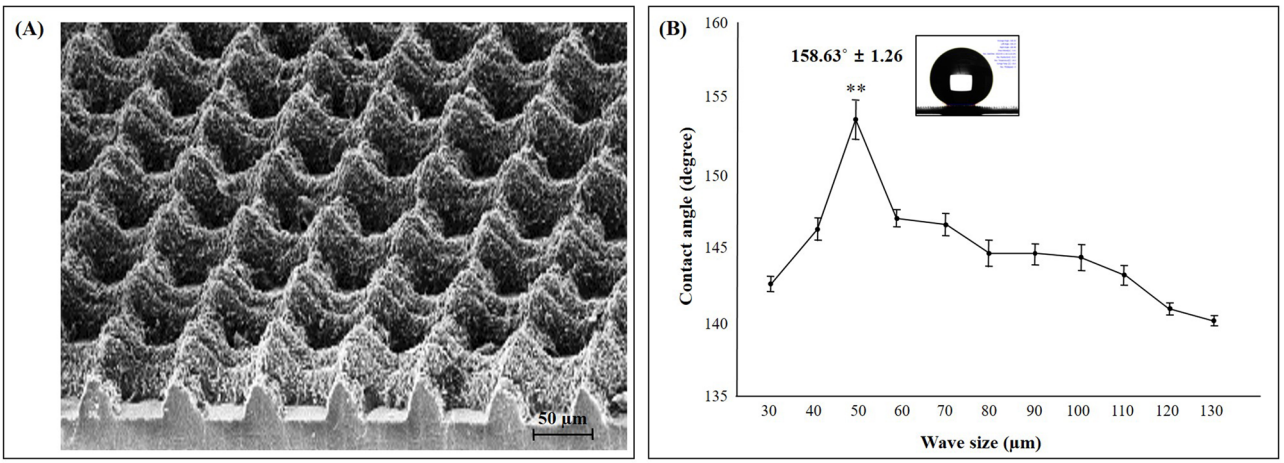

Fig. 5 Evaluation of material surface contact angle variation with the wave size in the Grid. Representative SEM image of the Grid (**A**), changes in surface contact angle based on wave size in the Grid (**B**). The indicated values are means ± SD ($n = 3$), $^{**}p < 0.01$. *P* values are statistical values corresponding to the wave size of 30 μm

contact angle decreased for a wave size of 60 μm (146.9° ± 0.42) and continued to decrease until a wave size of 110 μm (143.8° ± 0.46) (Fig. 5B).

3.5 Evaluation of initial cellular response to surface modified material

The change in the contact area between the cell culture medium and surface of the material modified by HFLS was validated by the degree of spreading of the cell culture medium. Consequently, the instant the culture medium was loaded onto the surface (0 h), it spread over the material surface on the Line, and the spreading gradually increased over time until it was nearly spread over the entire material surface in 24 h. Conversely, in the case of the Grid, the extent of spreading of the culture medium on the material surface was relatively narrow compared to that of the None and the Line, and did not spread all over the material surface even after 24 h (Fig. 6). This experiment could not be quantified because it was a simple qualitative result in the liquid state. Based on these results, the stained cells attached initially to the material surface were imaged using a

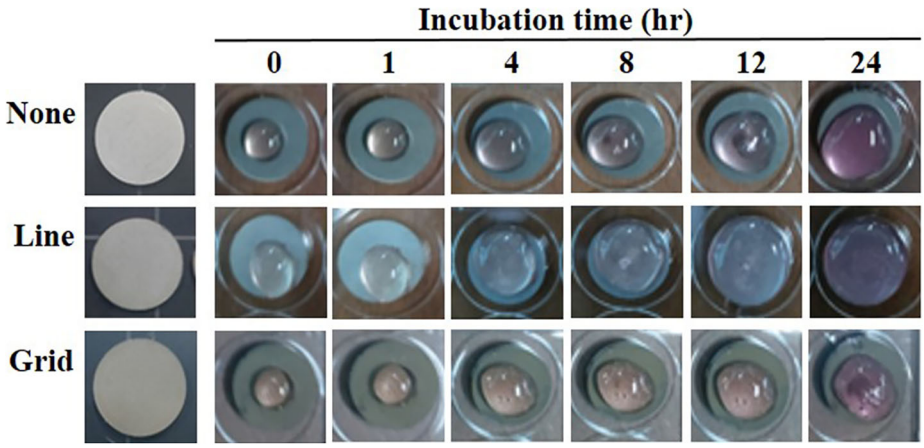

Fig. 6 Comparison of cell culture medium spreading on modified material surface. Images depicting spread behavior of cell culture medium on three kinds of titanium surface modified by HFLS after 24 h

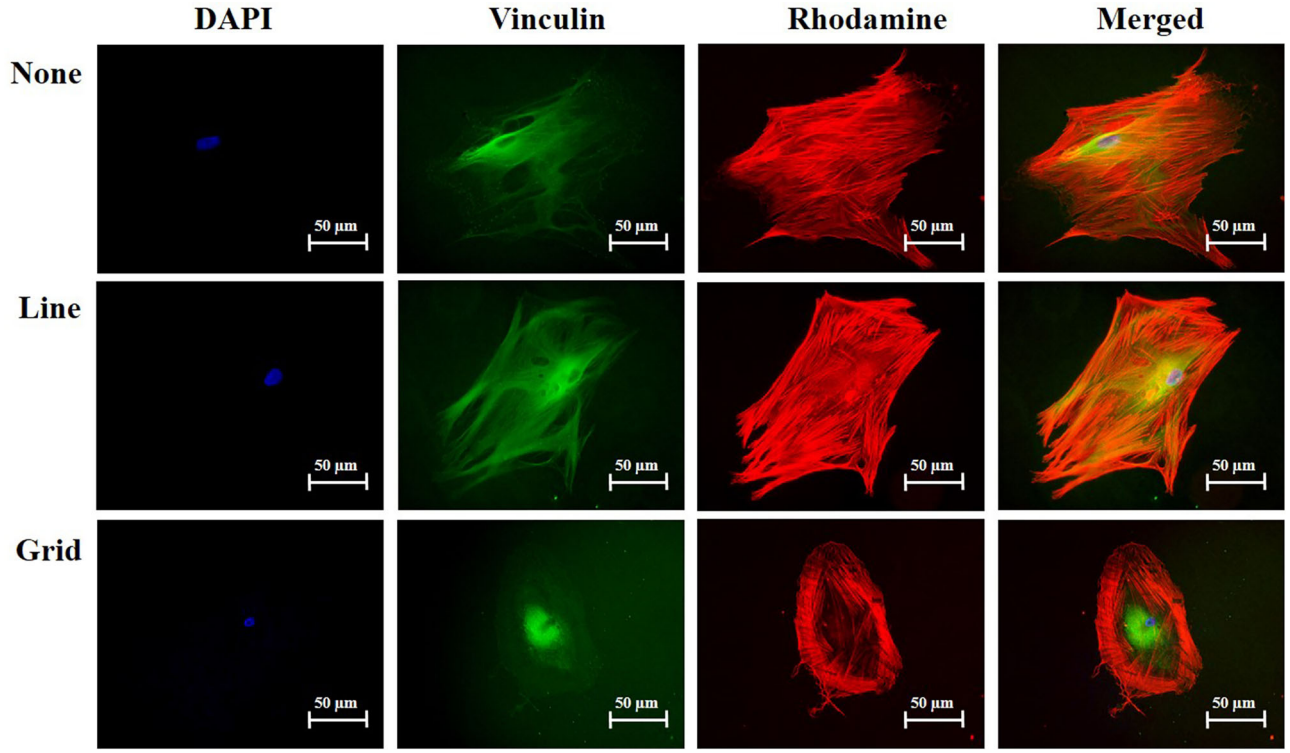

Fig. 7 Representative images of fluorescence microscope for initial focal cell adhesion. HGF is cultured for 4 h to observe the focal adhesion on PS surface. DAPI to label nucleic acids in the nucleus (blue), vinculin (green), and rhodamine-phalloidin to label actin (red) in HGF are stained as described in the material and method section. The images are represented by merging three images

fluorescence microscope. Although similar to that in the None group, the cytoplasmic area in the Line was significantly wider than that in the Grid. In addition, cell filopodia in the Line was more copious and elongated than those in the Grid, which was rarely observed (Fig. 7).

3.6 Investigation of cell migration and proliferation on material surfaces

Cell migration and proliferation were evaluated to determine the mid-phase cellular responses. A specific area (~12.0 ± 1.05 mm^2) of the cell monolayer on the culture dish was created as cell-empty space, and the extent to which cells migrated and filled the empty space was observed after 24 h of cultivation (Fig. 8A). The cell migration rates in the None and the Grid were ~63.5 ± 14.21% and 13.6 ± 22.36%, respectively. In contrast, the space where the cell was empty in the Line was filled with migrating cells to the extent that the cell migration rate could not be measured ($p < 0.01$; Fig. 8B). It exhibited a typical cell proliferation pattern in the None group, wherein cells increased with culture time and reached saturation at a specific time. This cell proliferation

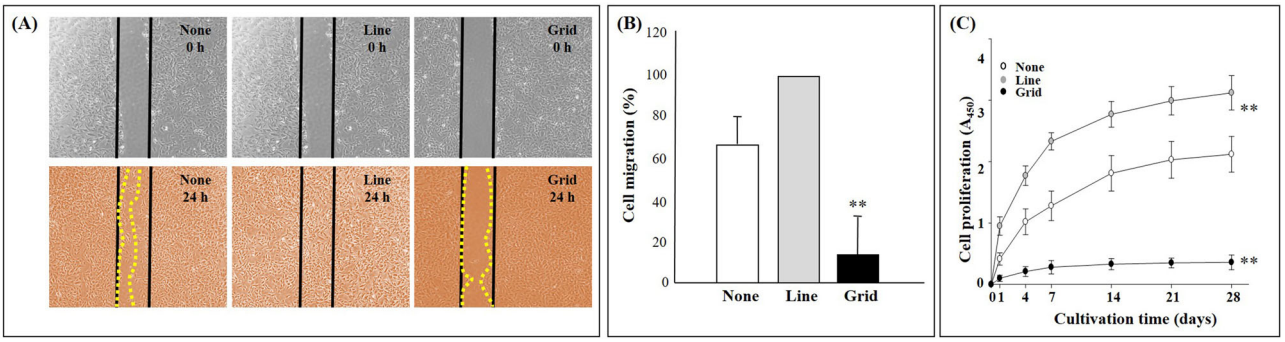

Fig. 8 Evaluation of cellular responses on modified PS surface. Representative images of cell migration for 24 h (**A**), quantitative analysis of cell migration (**B**), and cell proliferation (**C**). The thick black line indicates the initially scratched area (cell-empty space), and the yellow dotted line indicates the boundary between cell-empty space and area filled with cell after 24 h of cell migration. The indicated values are means ± SD ($n = 3$), $^{**}p < 0.01$. *P* values are statistical values compared to the None

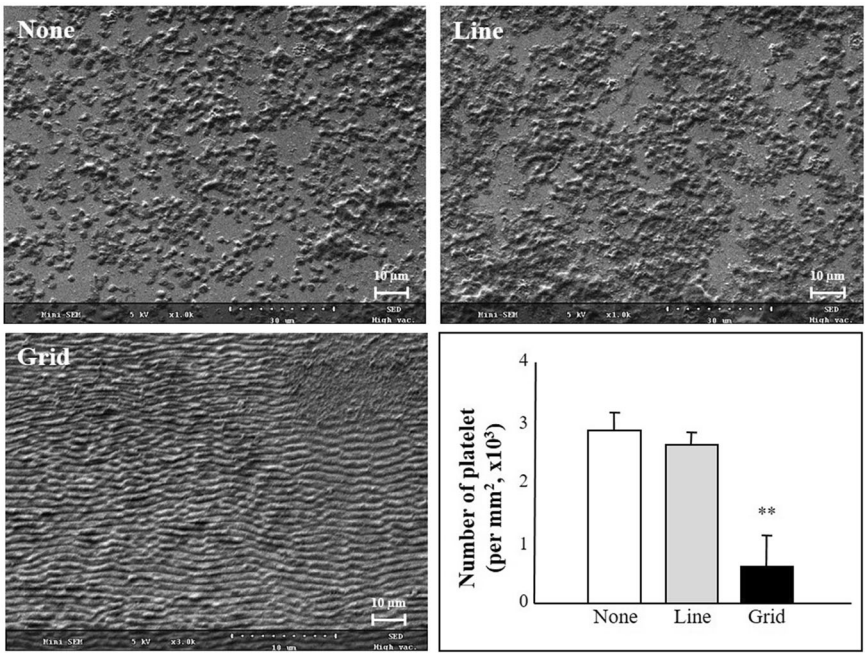

Fig. 9 Evaluation of platelet adhesion on modified material surface. Representative images and quantitative evaluations of platelets attached to each material surface. The indicated values are means ± SD ($n = 3$), $^{**}p < 0.01$. *P* values are statistical values compared to the None

pattern significantly increased in the Line from days 1 to 28 (an average increase of 58.6 ± 12.63% compared to that of the None, $p < 0.01$). Conversely, cell proliferation occurred minimally in the Grid (an average decrease of 82.3 ± 33.61% compared to that of the None, $p < 0.01$) (Fig. 8C).

3.7 Examination of platelet adhesion on material surfaces

Platelet adhesion examination was conducted to estimate the potential for thrombus formation. The number and distribution of attached platelets were similar in the None and Line (None, 2875 ± 236/mm^2; Line, 2638 ± 185/mm^2, p = ns). The platelets exhibited extended pseudopodia and several platelets were connected to each other. The attached platelets exhibited aggregation and distortion, and appeared to form clusters with swarm formation. In contrast, platelet adhesion in the Grid was significantly reduced compared with that in the other groups (Grid, 561 ± 879/mm^2, $p < 0.01$) and only minimal platelets were observed to be connected to each other (Fig. 9).

3.8 Measurement of drug holding capacity and in vitro drug release

To measure the total amount of PDS that could be incorporated into the material surface, the drug was loaded onto the material surface, as described earlier. The total drug amount on the material surface was measured, and the drug release pattern over time was expressed as a percentage of the total drug amount. The drug incorporated into the None group was detected at trace levels owing to wash-out, and

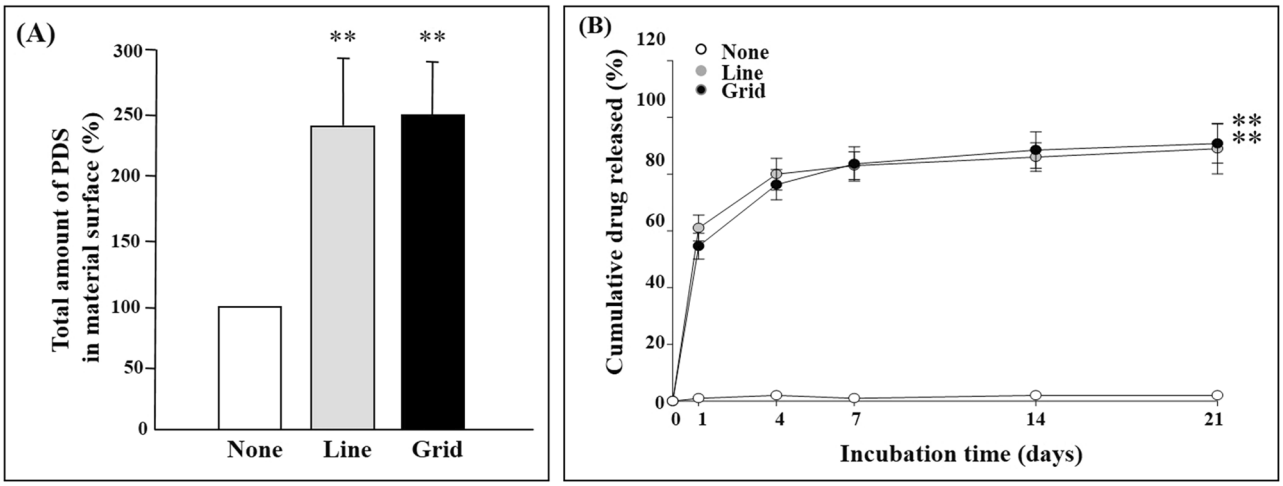

Fig. 10 Comparison of drug holding capacity and release between two of equipment. Total amount of PDS holding in materials (**A**) and its cumulative release from the materials (**B**) are presented. The indicated values are means ± SD ($n = 3$), $^{**}p < 0.01$. *P* values are statistical values compared to the None

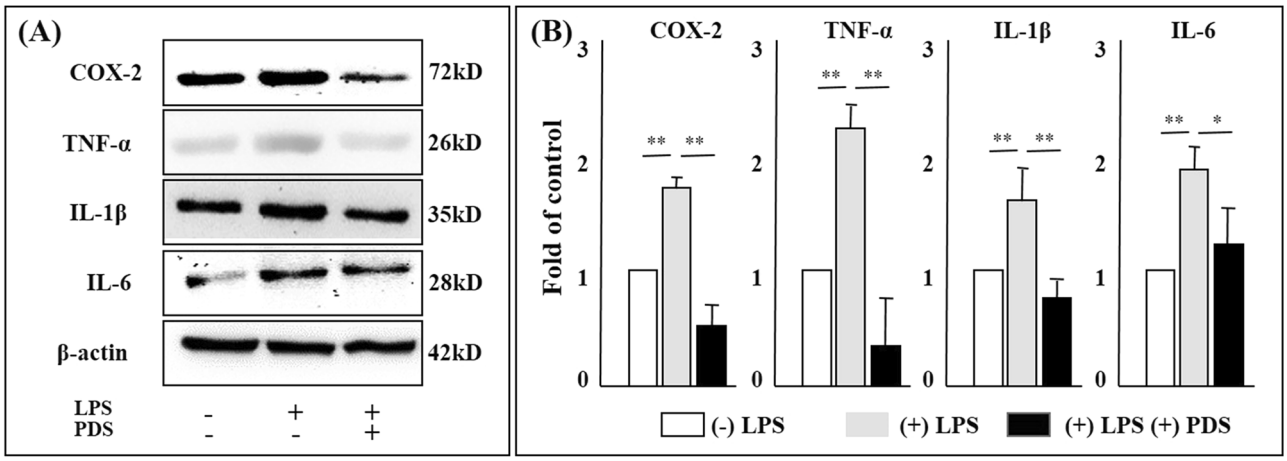

Fig. 11 Verification of the function of the released PDS from material by western blotting analysis. After activating various inflammatory cytokines by treating RAW 264.7 macrophages with LPS, the changes in response to the released PDS are represented (**A**). Expression levels are quantified using Gel-Pro software, and protein amounts are normalized to the intensity of control (**B**). The indicated values are means ± SD ($n = 3$), $^{*}p < 0.05$, $^{**}p < 0.01$

the drug incorporated into the Line and the Grid groups significantly increased statistically compared to that in the None group (Line, 238.5 ± 72.65%; Grid, 241.6 ± 61.28%, $n = 3$, $p < 0.01$) (Fig. 10A). Approximately 60% of the drug incorporated into the material surface was released on the first day, more than 80% was released on the 7 d, and almost no drug release occurred until day 21 (Fig. 10B).

3.9 Verification of the function of drug released from the material surface

The functionality of the drug released from the material surface was investigated based on the inflammatory effects of PDS. Western blot analysis demonstrated that the expression levels of inflammatory cytokines, including cyclooxygenase-2 (COX-2), tumor necrosis factor-α (TNF-α), interleukin (IL1-β), and IL-6, were significantly increased following LPS stimulation (Fig. 11A). However, the expression levels were substantially reduced following the release of PDS from the material surface. {Cox-2; 72.7 ± 8.45% ($p < 0.01$), TNF-α; 82.7 ± 13.6% ($p < 0.01$), IL-1β; 49.7 ± 9.85% ($p < 0.01$), and IL-6; 34.9 ± 11.05% ($p < 0.05$), respectively} (Fig. 11B).

4 Discussion

The newly developed laser equipment introduced in this study successfully addressed the limitations of conventional equipment, such as slow processing speeds and challenges

in achieving precision processing. This equipment combines high-speed processing, achieved via laser beam scanning using a high-speed rotating mirror along the X- and Y-axes of the scanner, with high-focus and high-precision processing, enabled by moving the stage while maintain the fixed laser beam using the objective lens type.

These two processing methods were combined by applying relay optics, enabling parallel light to focus at one point, thereby minimizing potential damage to the objective lens caused by the laser beam (Fig. 1) [19]. For both the Si wafer and silica, the results of HFLS irradiated once with a vibration beam were similar to those of 24 repetitions using conventional equipment processing. However, for PCB, which is widely used in semiconductor applications, the processing efficiency of HFLS was lower than that of the Si wafer, and silicon was processed by HFLS (HFLS: objective lens = 1:4 ~ 6 times repeated processing). Despite material-dependent variations in laser processing outcomes, HFLS demonstrated better processing efficiency, convenience, and overall performance compared with that of conventional equipment (Fig. 2).

The PS surfaces used in cell experiments were freely modified into the Line or the Grid using HFLS (Fig. 3). Although depth measurements using SEM were inconclusive, attempts to measure processing depth employing an atomic force microscope (AFM) also failed because it exceeded the measurement range of the cantilever of AFM (4 μm) (data not shown). However, it is estimated that the processing depth exceeds 4 μm, which is the measurement range of cantilever and, based on the results presented in Fig. 2, it likely reaches tens of micrometers. The hydrophilicity of the material surface significantly increased in the Line group, whereas hydrophobicity was markedly enhanced in the Grid group, compared with the untreated (None) surface. These results were consistent between two-dimensional specimens and three-dimensional dental implant surfaces (Fig. 4). Although previous studies indicate that wettability can be influenced by multiple factors including surface shape, roughness, protrusion height [41], and surface energy [42], the overall trends in our HFLS-modified surfaces were reproducible and consistent with the observed biological responses. Thus, the distinction between None, Line, and Grid surfaces reflects deliberate and controllable modifications, rather than inconsistencies. However, the variation in surface properties observed in the present study closely align with the physical theory that water penetration and surface wettability are influenced by the Cassie–Baxter and Wenzel states [44]. This is evident when additional axial processing is applied to previously processed material (such as the Grid in this study) and nanoscale features are incorporated into micropores [43]. To demonstrate the engineering superiority of HFLS in biological applications, detailed investigation into the variation in surface properties with wave size is essential. The contact angle of the biomaterial surface increased to 158.63° ± 1.26 at a wave size of 50 μm (Fig. 5).

Compared with the untreated (None) surface, the Line pattern significantly increased hydrophilicity, while the Grid pattern increased hydrophobicity. Although multiple parameters such as surface roughness and topography can influence wettability, the observed trends in our HFLS-modified surfaces were consistent and reproducible. Thus, the variation between None, Line, and Grid surfaces reflects distinct and controllable modifications rather than inconsistencies. Given that typical cell sizes are less than 100 μm, a wave size of ~50 μm appears optimal for enhancing surface property modification and reactivity of the cells. In addition, modification may inhibit substances that may induce a negative clinical prognosis, such as platelets, inflammatory cells, and bacteria, while improving the accessibility of clinically positive substances, such as endothelial cells, fibroblasts, and osteogenic cells. Therefore, the ability to regulate surface modification using the HFLS equipment indicates that it is likely an approach to achieving the desired pathological outcomes. However, additional bacterial studies are required to substantiate this hypothesis.

The interaction between the material and culture medium establishes the foundational environment for cellular responses. This study demonstrated that the PS surface optimized for cell culture was optimally modified by HFLS (Fig. 3). Hydrophilic surfaces (the Line) allowed the culture to spread more efficiently, whereas hydrophobic surfaces (the Grid) exhibited limited spread, indirectly indicating the possibility of cell-material contact (Fig. 6). To confirm this, initial focal cell adhesion was investigated via fluorescence microscopy using a staining technique. Rhodamine, a dye used for cytoplasmic visualization in this study, and vinculin, a protein associated with initial focal cell adhesion located on the cytoplasmic side [45], were minimally observed in the Grid surface (Fig. 7). The absence of filopodia [46], which are involved in cell movement in the Grid, seemed to affect cell migration (Fig. 8B) and cell proliferation (Fig. 8C). When implanted, a biomaterial first contacts blood, body fluids, and cells. The clinical outcome depends on the site, duration, and type of contact. Therefore, controlling the surface properties of biomaterials can be used for predicting and improving clinical prognosis.

This study confirmed that the surface morphology of biomaterials determines their properties (Fig. 4) and can affect cell fate (Figs. 8 and 9) [47]. These initial or mid-phase cellular responses can be interpreted as precursor processes that can be linked to pathological outcomes, such as wound healing, immune responses, and bone regeneration, which are achieved through preemptive adhesion of endothelial or osteogenic cells to epithelial cells, inflammatory cells, and platelets that can compete for adhesion to

the biomaterial surface [48, 49]. Biomaterials are foreign materials that can lead to thrombotic events. Therefore, the interaction between platelets and biomaterials during the initial phase of implantation is a key event that determines the fate of the blood coagulation cascade [50]. This cascade begins with platelets adhering to the material surface, followed by aggregation and coagulate. Subsequently, the platelets transition into a star-shaped morphology. Eventually the platelets rupture, exposing the substances involved in thrombosis contained within them [51]. As shown in Fig. 9, the frequencies of platelet adhesion, aggregation, and other thrombosis-related morphologies in the Grid were significantly reduced compared with those in the None and the Line. Therefore, a Grid-shaped surface modification may be advantageous for reducing thrombosis-related issues. Our findings suggest a correlation between surface wettability and biological responses. Hydrophilic surfaces (Line, low contact angle) promoted spreading, adhesion, and proliferation of human gingival fibroblasts. In contrast, hydrophobic surfaces (Grid, high contact angle) reduced cell adhesion and proliferation, while also markedly decreasing platelet adhesion. These results imply that both cell and platelet adhesion share a similar dependency on surface wettability, although further studies are needed to elucidate the underlying mechanisms. Based on prior studies, we hypothesized that surface modification imparted materials with porosity [10] and roughness [29], thereby increasing the drug-holding capacity. As shown in Fig. 10A, the drug present on the smooth surface was washed out and depleted rapidly following implantation. However, any surface was modification (the Line or the Grid in this study), significantly increased the amount of drug-incorporated material. The release pattern of the holding drug in this study aligns with that observed in our previous study [10], which can be interpreted as a burst release pattern rather than a washed-out pattern, where the drug disappears immediately after the biomaterial is implanted in the body.

For sustained release applications, such as osteogenesis, further studies are needed. In particular, barriers or chemical bonding may help delay drug release. This is an important requirement for biomaterials serving as drug delivery carriers, because the drug released from the material surface maintains its original function. In this study, we indirectly demonstrated in vitro that the HFLS-modified material surface maintained its anti-inflammatory effects after the delivery and release of PDS into the body (Fig. 11). Although the terms M1 and M2, which describe the inflammatory mechanism, may not fully capture drug delivery capacities of biomaterials [52], considering the types of cytokines suppressed and referring to our previous study [53], PDS on the material surface is associated with M1 macrophages rather than M2 macrophages.

5 Conclusions

In this study, a new type of advanced laser equipment was developed by integrating the advantages of conventional laser equipment. This equipment enabled rapid and precise surface modification of biomaterials than that by conventional laser equipment. The material surface was modified to be hydrophilic or hydrophobic, and biological functions, such as cell response, drug delivery efficacy, and anti-inflammatory effects, were validated. Therefore, the newly developed laser equipment proposed in this study offers a promising approach for achieving tissue engineering functions such as modifying biomaterial surfaces into desired shapes, improving cytocompatibility, and enhancing drug delivery capacity. Furthermore, it holds significant potential in facilitating clinical accessibility serving as a versatile device capable of addressing diverse biomedical needs.

Acknowledgements This work was supported by the National Research Foundation of Korea grant funded by the Korean Government (MSIT) (No. RS-2023-00222390).

Compliance with ethical standards

Conflict of interest The authors declare no competing interests.

Publisher's note Springer Nature remains neutral with regard to jurisdictional claims in published maps and institutional affiliations.

References

1. Wei Y, Cheng Y, Wei H, Wang Y, Zhang X, Miron RJ, et al. Development of a super-hydrophilic anaerobic tube for the optimization of platelet-rich fibrin. Platelets. 2024;35:1–12.
2. Mystkowska J, Niemirowicz-Laskowska K, Lysik D, Tokajuk G, Dabrowski JR, Bucki R. The role of oral cavity biofilm on metallic biomaterial surface destruction-corrosion and friction aspects. Int J Mol Sci. 2018;19:743.
3. Thevenot P, Hu W, Tang L. Surface chemistry influences implant biocompatibility. Curr Top Med Chem. 2008;8:270–80.
4. Park KM, Lee HJ, Koo KT, Ben Amara H, Leesungbok R, Noh K, et al. Oral soft tissue regeneration using nano controlled system

inducing sequential release of trichloroacetic acid and epidermal growth factor. Tissue Eng Regen Med. 2020;17:91–103.
5. Vas WJ, Shah M, Al Hosni R, Owen HC, Roberts SJ. Biomimetic strategies for fracture repair: Engineering the cell microenvironment for directed tissue formation. J Tissue Eng. 2017;8:1–14.
6. Cao Y, Su B, Chinnaraj S, Jana S, Bowen L, Charlton S, et al. Nanostructured titanium surfaces exhibit recalcitrance towards staphylococcus epidermidis biofilm formation. Sci Rep. 2018;8:1071.
7. Jaggessar A, Mathew A, Wang H, Tesfamichael T, Yan C, Yarlagadda PK. Mechanical, bactericidal and osteogenic behaviours of hydrothermally synthesised TiO(2) nanowire arrays. J Mech Behav Biomed Mater. 2018;80:311–9.
8. Ghosh S, Niu S, Yankova M, Mecklenburg M, King SM, Ravichandran J, et al. Analysis of killing of growing cells and dormant and germinated spores of bacillus species by black silicon nanopillars. Sci Rep. 2017;7:17768.
9. Hasan J, Raj S, Yadav L, Chatterjee K. Engineering a nanostructured "super surface" with superhydrophobic and superkilling properties. RSC Adv. 2015;5:44953–9.
10. Bae I, Lim KS, Park JK, Song JH, Oh SH, Kim JW, et al. Evaluation of cellular response and drug delivery efficacy of nanoporous stainless steel material. Biomater Res. 2021;25:30.
11. Hizal F, Zhuk I, Sukhishvili S, Busscher HJ, van der Mei HC, Choi CH. Impact of 3D hierarchical nanostructures on the antibacterial efficacy of a bacteria-triggered self-defensive antibiotic coating. ACS Appl Mater Interfaces. 2015;7:20304–13.
12. Dickson MN, Liang EI, Rodriguez LA, Vollereaux N, Yee AF. Nanopatterned polymer surfaces with bactericidal properties. Biointerphases. 2015;10:021010.
13. Doll PW, Wolf M, Guttmann M, Thelen R, Ahrens R, Spindler B, et al. Initial bacterial adhesion properties of anodically oxidized Ti(6)Al(4)V. Annu Int Conf IEEE Eng Med Biol Soc. 2019;2019:6476–80.
14. Bae IH, Jeong MH, Lim KS, Park DS, Shim JW, Park JK, et al. Novel polymer-free everolimus-eluting stent fabricated using femtosecond laser improves re-endothelialization and anti-inflammation. Sci Rep. 2018;8:7383.
15. Mai EL, Lian IB, Chang DC. Assessment of contrast sensitivity loss after intrastromal femtosecond laser and LASIK procedure. Int J Ophthalmol. 2016;9:1798–801.
16. Kuetemeyer K, Rezgui R, Lubatschowski H, Heisterkamp A. Influence of laser parameters and staining on femtosecond laser-based intracellular nanosurgery. Biomed Opt Express. 2010;1:587–97.
17. Boutopoulos C, Bergeron E, Meunier M. Cell perforation mediated by plasmonic bubbles generated by a single near infrared femtosecond laser pulse. J Biophotonics. 2016;9:26–31.
18. Jeon H, Koo S, Reese WM, Loskill P, Grigoropoulos CP, Healy KE. Directing cell migration and organization via nanocrater-patterned cell-repellent interfaces. Nat Mater. 2015;14:918–23.
19. Kim JH, Park KH, IB Solution Co., Ltd. Detachable optical device for adjusting beam focusing speed of laser scanner. Koreanpatent KR10-2021-0042230A. Published 2021 Apr 19.
20. Zhou S, Liu Y, Yu X, Wang D, Wang X, Li Q. Bidirectional elastic PTFE small diameter artificial blood vessel grafts and surface antithrombotic functionalized construction. ACS Appl Bio Mater. 2024;7:6985–97.
21. Kulakowski D, Phansalkar RM, Leme-Kraus AA, McAlpine J, Chen SN, Pauli GF, et al. Galloylated proanthocyanidins in dentin matrix exhibit biocompatibility and induce differentiation in dental stem cells. J Bioact Compat Polym. 2022;37:220–30.
22. Win HK, Caldera AE, Maresh K, Lopez J, Rihal CS, Parikh MA, et al. Clinical outcomes and stent thrombosis following off-label use of drug-eluting stents. JAMA. 2007;297:2001–9.
23. Daemen J, Wenaweser P, Tsuchida K, Abrecht L, Vaina S, Morger C, et al. Early and late coronary stent thrombosis of sirolimus-eluting and paclitaxel-eluting stents in routine clinical practice: data from a large two-institutional cohort study. Lancet. 2007;369:667–8.
24. Bae IH, Park DS, Lee SY, Jang EJ, Shim JW, Lim KS, et al. Bilirubin coating attenuates the inflammatory response to everolimus-coated stents. J Biomed Mater Res B Appl Biomater. 2018;106:1486–95.
25. Shim JW, Bae IH, Park DS, Lim KS, Lee SY, Jang EJ, et al. Evaluation of ion implantation for anti-thrombogenic coronary stent in vitro and in vivo. J Indust Eng Chem. 2017;54:290–7.
26. Bae IH, Yun KD, Kim HS, Jeong BC, Lim HP, Park SW, et al. Anodic oxidized nanotubular titanium implants enhance bone morphogenetic protein-2 delivery. J Biomed Mater Res B Appl Biomater. 2010;93:484–91.
27. Yun KD, Yang Y, Lim HP, Oh GJ, Koh JT, Bae IH, et al. Effect of nanotubular-micro-roughened titanium surface on cell response in vitro and osseointegration in vivo. Mater Sci Eng C. 2010;30:27–33.
28. Shim JW, Bae IH, Park DS, Lee SY, Jang EJ, Lim KS, et al. Hydrophilic surface modification of coronary stent using an atmospheric pressure plasma jet for endothelialization. J Biomater Appl. 2018;32:1083–9.
29. Bae IH, Choe HC, Ahn SG, Kim BH. Effect of microarchitectural surface of polycaprolactone modified by reactive ion etching on osteogenic differentiation. Appl Surf Sci. 2023;610:155571.
30. Curtis A, Wilkinson C. Topographical control of cells. Biomaterials. 1997;18:1573–83.
31. Kasemo B, Gold J. Implant surfaces and interface processes. Adv Dent Res. 1999;13:8–20.
32. Dobbenga S, Fratila-Apachitei LE, Zadpoor AA. Nanopattern-induced osteogenic differentiation of stem cells - a systematic review. Acta Biomater. 2016;46:3–14.
33. Lee SY, Bae IH, Park DS, Jang EJ, Shim JW, Lim KS, et al. Prednisolone- and sirolimus-eluting stent: Anti-inflammatory approach for inhibiting in-stent restenosis. J Biomater Appl. 2016;31:36–44.
34. Park DS, Bae IH, Jeong MH, Lim KS, Sim DS, Hong YJ, et al. In vitro and in vivo evaluation of a novel polymer-free everolimus-eluting stent by nitrogen-doped titanium dioxide film deposition. Mater Sci Eng C Mater Biol Appl. 2018;91:615–23.
35. Jang S, Jeong MH, Lim KS, Bae IH, Park JK, Park DS, et al. Effect of stents coated with artemisinin or dihydroartemisinin in a porcine coronary restenosis model. Korean Circ J. 2017;47:115–22.
36. Bae IH, Jeong MH, Park DS, Lim KS, Shim JW, Kim MK, et al. Mechanical and physio-biological properties of peptide-coated stent for re-endothelialization. Biomater Res. 2020;24:4.
37. Ribichini F, Joner M, Ferrero V, Finn AV, Crimins J, Nakazawa G, et al. Effects of oral prednisone after stenting in a rabbit model of established atherosclerosis. J Am Coll Cardiol. 2007;50:176–85.
38. Liang CC, Park AY, Guan JL. In vitro scratch assay: a convenient and inexpensive method for analysis of cell migration in vitro. Nat Protoc. 2007;2:329–33.
39. Bae IH, Park IK, Park DS, Lee H, Jeong MH. Thromboresistant and endothelialization effects of dopamine-mediated heparin coating on a stent material surface. J Mater Sci Mater Med. 2012;23:1259–69.
40. Salonen J, Laitinen L, Kaukonen AM, Tuura J, Bjorkqvist M, Heikkila T, et al. Mesoporous silicon microparticles for oral drug delivery: loading and release of five model drugs. J Control Rel. 2005;108:362–74.
41. Josyula T, Kumar Malla L, Thomas TM, Kalichetty SS, Sinha Mahapatra P, Pattamatta A. Fundamentals and applications of surface wetting. Langmuir. 2024;40:8293–326.
42. Tarasevich YI. The surface energy of hydrophilic and hydrophobic adsorbents. Colloid J. 2007;69:212–20.

43. Giacomello A, Meloni S, Chinappi M, Casciola CM. Cassie-Baxter and Wenzel states on a nanostructured surface: phase diagram, metastabilities, and transition mechanism by atomistic free energy calculations. Langmuir. 2012;28:10764–72.
44. Yin L, Zhu L, Wang Q, Ding J, Chen Q. Superhydrophobicity of natural and artificial surfaces under controlled condensation conditions. ACS Appl Mater Interfaces. 2011;3:1254–60.
45. Otto JJ. Vinculin. Cell Motil Cytoskeleton. 1990;16:1–6.
46. Mattila PK, Lappalainen P. Filopodia: molecular architecture and cellular functions. Nat Rev Mol Cell Biol. 2008;9:446–54.
47. Anselme K. Osteoblast adhesion on biomaterials. Biomaterials. 2000;21:667–81.
48. Xu C, Yang F, Wang S, Ramakrishna S. In vitro study of human vascular endothelial cell function on materials with various surface roughness. J Biomed Mater Res A. 2004;71:154–61.
49. Wan Y, Wang Y, Liu Z, Qu X, Han B, Bei J, et al. Adhesion and proliferation of OCT-1 osteoblast-like cells on micro- and nano-scale topography structured poly(L-lactide). Biomaterials. 2005;26:4453–9.
50. Suzuki Y, Iwaki M, Takahashi N, Yotoriyama T, Kurotobi K, Ujiie H, et al. In vitro and in vivo study of He+ ion irradiated collagen for development of small diameter stent graft material. Nucl Instrum Meth B. 2005;232:353–7.
51. Hansi C, Arab A, Rzany A, Ahrens I, Bode C, Hehrlein C. Differences of platelet adhesion and thrombus activation on amorphous silicon carbide, magnesium alloy, stainless steel, and cobalt chromium stent surfaces. Catheter Cardiovasc Inter. 2009;73:488–96.
52. Varga T, Mounier R, Horvath A, Cuvellier S, Dumont F, Poliska S, et al. Highly dynamic transcriptional signature of distinct macrophage subsets during sterile inflammation, resolution, and tissue repair. J Immunol. 2016;196:4771–82.
53. Bae I, Kim BH. Drug release control and anti-inflammatory effect of biodegradable polymer surface modified by gas phase chemical functional reaction. Biomed Mater. 2024;19:025045.